

Instability of the current sheet in the Earth's magnetotail with normal magnetic field

N. Bessho and A. Bhattacharjee

Citation: *Physics of Plasmas* (1994-present) **21**, 102905 (2014); doi: 10.1063/1.4899043

View online: <http://dx.doi.org/10.1063/1.4899043>

View Table of Contents: <http://scitation.aip.org/content/aip/journal/pop/21/10?ver=pdfcov>

Published by the [AIP Publishing](#)

Articles you may be interested in

[Nonlinear evolution of three-dimensional instabilities of thin and thick electron scale current sheets: Plasmoid formation and current filamentation](#)

Phys. Plasmas **21**, 072306 (2014); 10.1063/1.4887279

[Collisionless instability of thin current sheets in the presence of sheared parallel flows](#)

Phys. Plasmas **15**, 082901 (2008); 10.1063/1.2968459

[Modeling of ion heating from viscous damping of reconnection flows in the reversed field pinch](#)

Phys. Plasmas **15**, 062511 (2008); 10.1063/1.2937121

[Small-scale reconnection due to lower-hybrid drift instability in current sheets with sheared fields](#)

Phys. Plasmas **12**, 012320 (2005); 10.1063/1.1830015

[Influence of the lower hybrid drift instability on the onset of magnetic reconnection](#)

Phys. Plasmas **11**, 4489 (2004); 10.1063/1.1778744

A collection of five pieces of Pfeiffer Vacuum equipment, including a red turbopump, a silver turbopump, a silver turbopump with a control panel, a red turbopump with a long shaft, and a silver chamber component.

 Vacuum Solutions from a Single Source

- Turbopumps
- Backing pumps
- Leak detectors
- Measurement and analysis equipment
- Chambers and components

PFEIFFER  **VACUUM**

Instability of the current sheet in the Earth's magnetotail with normal magnetic field

N. Bessho^{1,a)} and A. Bhattacharjee²

¹Department of Astronomy, University of Maryland, College Park, Maryland 20742, USA and Heliophysics Science Division, NASA Goddard Space Flight Center, Maryland 20771, USA

²Center for Heliophysics, Department of Astrophysical Sciences and Princeton Plasma Physics Laboratory, Princeton University, New Jersey 08543, USA

(Received 11 June 2014; accepted 7 October 2014; published online 24 October 2014)

Instability of a current sheet in the Earth's magnetotail has been investigated by two-dimensional fully kinetic simulations. Two types of magnetic configuration have been studied; those with uniform normal magnetic field along the current sheet and those in which the normal magnetic field has a spatial hump. The latter configuration has been proposed by Sitnov and Schindler [Geophys. Res. Lett. **37**, L08102 (2010)] as one in which ion tearing modes might grow. The first type of configuration exhibits electron tearing modes when the normal magnetic field is small. The second type of configuration exhibits an instability which does not tear or change the topology of magnetic field lines. The hump in the initial configuration can propagate Earthward in the nonlinear regime, leading to the formation of a dipolarization front. Secondary magnetic islands can form in regions where the normal magnetic field is very weak. Under no conditions do we find the ion tearing instability. © 2014 AIP Publishing LLC. [<http://dx.doi.org/10.1063/1.4899043>]

I. INTRODUCTION

A tearing instability, by definition, is one in which magnetic field lines are torn or broken, leading to the reconfiguration of a laminar field-reversed configuration into one with multiple islands. The collisionless tearing instability of the Earth's magnetotail in the presence of a B_z field has had a long and vexing history. It began with the identification of the electron tearing mode by Coppi *et al.*¹ in a magnetotail without B_z , with electron inertia providing the mechanism for breaking field lines. However, it was shown later that the electron tearing instability is stabilized by magnetized electrons due in the presence of a magnetic field B_z normal to the current sheet,²⁻⁴ which cannot be neglected in the Earth's magnetotail. By means of heuristic arguments, Schindler³ proposed that the electron tearing instability is replaced by the ion tearing instability since the ions remain unmagnetized despite the presence of B_z . This led to significant debate in the magnetospheric physics community, with some questioning the very existence of the instability. Lembege and Pellat⁵ argued that the ion tearing mode is stable because of the density compression in the current sheet. Pellat *et al.*⁶ discussed that the ion tearing instability cannot exist even considering the effect of pitch angle scattering or the stochastic changes of the adiabatic invariant of electrons,^{7,8} because the effects of density compression are barely affected by such mechanisms.⁹ Wang and Bhattacharjee¹⁰ argued that only the electron tearing mode exists when B_z becomes small, and no tearing instability is possible in the presence of significant B_z because of the strongly stabilizing effects of ion compression in the Earth's magnetotail. Pritchett *et al.*¹¹ and Pritchett¹² performed kinetic simulations and showed that the ion tearing instability is suppressed

when electron physics (magnetization by B_z) is included. Harrold *et al.*¹³ argued that there is no topological change in the magnetic field by the instability when there is a normal magnetic field; therefore, such a magnetic geometry is intrinsically resilient to the tearing instability independent of the mechanism that breaks field lines.

Recently, there has been a revival of this debate, stimulated in part by new observations of the so-called dipolarization front by THEMIS spacecraft. Sitnov and Schindler¹⁴ have recently proposed a new magnetic field configuration that they claim can destabilize the ion tearing mode. In this configuration, there is a hump of the normal magnetic field B_z in a current sheet. Sitnov and Swisdak¹⁵ and Sitnov *et al.*¹⁶ have studied such a magnetic configuration by means of two-dimensional (2D) particle-in-cell (PIC) simulations and suggest that as the hump of B_z moves earthwards, a dipolarization front is eventually formed. They argue that the formation of the dipolarization front is facilitated by the ion tearing instability.

In this paper, consistent with our earlier results, we demonstrate by means of fully kinetic, 2D PIC simulations that there is no ion tearing instability in the magnetotail in the presence of a significant B_z -field, notwithstanding the novel configuration(s) considered by Sitnov and co-workers. The only linear tearing instability that can occur in a magnetotail is the electron tearing instability, and that too when the magnitude of B_z is very small. However, the configuration proposed by Sitnov and co-workers exhibits an instability which does not tear or change the topology of magnetic field lines and yet, in a late nonlinear stage leads to the reduction of B_z to small and negative values that can support reconnection and the formation of secondary islands. However, the formation of the dipolarization front itself does not necessarily involve reconnection.

The following is a layout of this paper. In Sec. II, we describe our simulation method, initial conditions, and

^{a)}Electronic address: naoki.bessho@nasa.gov

plasma parameters. Unlike some other studies, we do not impose an external dawn-dusk electric field E_y in our study. In Sec. III, we show our simulation results. In Sec. IV, we conclude with a summary and a discussion of our findings.

II. SIMULATION METHOD

The details of the simulation code are described in Ref. 17. The simulation domain is in the x - z plane and given by $0 < x < 200w$ and $-12.5w < z < 12.5w$, where w is the sheet width at $x=0$. The magnetic field and density in the initial state have the following forms, and comprise an approximate solution of the Vlasov equation in a 2D generalized Harris sheet with a finite B_z :

$$B_x = -\frac{B_0}{g(x)} \tanh\left(\frac{z}{wg(x)}\right), \quad (1)$$

$$B_z = wB_0 \frac{g'(x)}{g(x)} \left[1 - \frac{z}{wg(x)} \tanh\left(\frac{z}{wg(x)}\right) \right], \quad (2)$$

$$n = \frac{n_0}{g(x)^2} \operatorname{sech}^2\left[\frac{z}{wg(x)}\right] + n_b + \epsilon(x, z), \quad (3)$$

where $g(x)$ is a function of x with $g(0) = 1$, $g'(x)$ is $dg(x)/dx$, n_b is the background density (with no drift in the y direction), and $\epsilon(x, z)$ is a function given by

$$\begin{aligned} \epsilon(x, z) = & \frac{n_0 g(x)^{j_2}}{g(x)^4} z^2 \operatorname{sech}^2\left[\frac{z}{wg(x)}\right] + n_0 w^2 \frac{g(x)'' g(x) - g(x)'^2}{g(x)^2} \\ & - n_0 w \frac{g(x)'' g(x) - 2g(x)'^2}{g(x)^3} z \tanh\left[\frac{z}{wg(x)}\right], \end{aligned} \quad (4)$$

which is derived by substituting Eqs. (1) and (2) into Ampere's law, $\partial B_x/\partial z - \partial B_z/\partial x = (4\pi ne/c)(v_{yi} - v_{ye})$. We use conditions, $B_0^2/8\pi = n_0(T_i + T_e)$, $|v_{di} - v_{de}| = (2c/weB_0)(T_i + T_e)$ and $v_{di}/v_{de} = -T_i/T_e$, where T_i and T_e are the ion and electron temperature, respectively, c is the speed of light, e is the elementary charge, and v_{di} and v_{de} represent the drift speed of ion and electron, respectively, in the y direction in drifting Maxwell distributions for particles. We consider two types of $g(x)$ (Case I and Case II). In Case I,

$$g(x) = \exp(\epsilon_1 x/w), \quad (5)$$

where ϵ_1 is a positive constant. In this type of simulation, B_z along $z=0$ is uniform, and it is equal to $\epsilon_1 B_0$, as seen in Fig. 1(a). This configuration is the same as in Pritchett *et al.*¹¹ and Pritchett,¹² and we can neglect $\epsilon(x, z)$ in the density n when $\epsilon_1 \ll 1$. In Case II,

$$g(x) = \exp(\epsilon_1 h(x/w)), \quad (6)$$

$$h(x/w) = x/w + (\alpha/\epsilon_2) \{1 + \tanh[\epsilon_2(x - x_0)/w]\}, \quad (7)$$

where ϵ_2 is a positive constant. In this type of simulation, B_z along $z=0$ has a hump, shown in Fig. 1(b). This is the case discussed by Sitnov and Schindler.¹⁴ Note that in Case II, $\epsilon(x, z)$ in the density n cannot be neglected even when $\epsilon_1 \ll 1$, and is needed to balance the $J_y \times B_z$ force by the pressure gradient along x . The magnetic configuration in

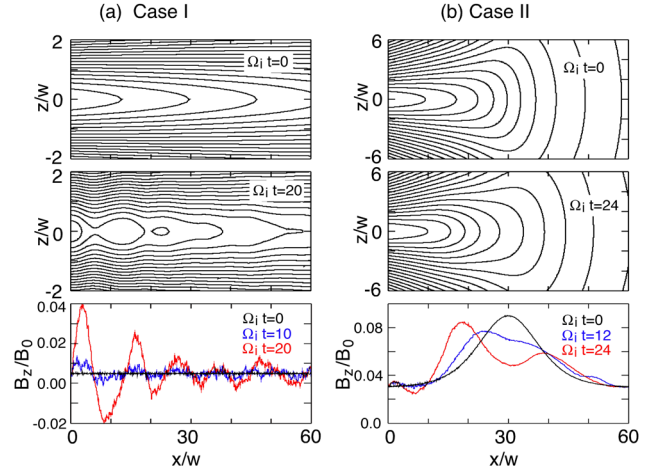


FIG. 1. (Top and middle) contours of magnetic flux function. (Bottom) time evolution of B_z along $z=0$. (a) Case I ($\epsilon_1 = 0.005$, $m_i/m_e = 25$). (b) Case II ($\epsilon_1 = 0.03$, $\epsilon_2 = 0.1$, $\alpha = 2.0$, $m_i/m_e = 100$).

Sitnov and Swisdak¹⁵ and in Sitnov *et al.*¹⁶ has left-right symmetry, and it is slightly different from Case II of our simulation. The configuration in Pritchett¹⁸ is similar to Case II.

Our boundary conditions are as follows. We impose conducting walls along z , and open boundaries along x (both at left and right), where light waves perpendicular to the boundaries can pass through without reflection. For implementing open boundary conditions, we follow the methodology discussed in Ref. 19. For particle injection from the boundaries, we calculate the particle number at one cell outside of the simulation box using Eq. (3) and obtaining $\partial n/\partial x$, and inject both the current sheet component and the background component, which are Maxwellian distributions. Note that in 2D configurations in which $B_z \neq 0$, Eqs. (1)–(4) are approximate solutions of the equilibrium state; therefore, particularly in high z regions, the deviation of these solutions from exact equilibrium solutions of the Vlasov-Maxwell system generates an initial perturbation in E_y which produces non-equilibrium flows which can interfere with the identification of a linear instability. To mitigate the effect of the initial perturbation, we set the z boundaries not too far from $z=0$, and wave-damping regions are placed near the conducting walls in the domain $9.6w < |z| < 12.5w$, where a damping factor between zero and unity is multiplied to the terms $-(4\pi/c)\mathbf{J} + \nabla \times \mathbf{B}$ in Ampere's law, where \mathbf{J} is the current density.

We use the following parameters: the sheet width $w = 0.5d_{i0}$, where d_{i0} is the ion skin depth based on the density n_0 , the temperature ratio $T_i/T_e = 5$ (the background plasma also has the same temperature and the same temperature ratio), the Alfvén speed v_A based on the density n_0 , and the magnetic field B_0 is 1/15 of the speed of light. We employ 2048 grid points in the x -direction, and 256 in the z -direction. We use the mass ratio m_i/m_e from 25 to 400 to determine the dependence of the instability on the mass ratio. We use a fixed number of particles to represent both the current sheet component and the background component at $t=0$ in all the runs, with a total of about 10^8 particles. For the background plasma (represented by n_b in Eq. (3)), we use about 131 particles per cell. For the current sheet component

of plasmas, the particle number at $x=0$ (represented by n_0) depends on the magnetic field configuration. For example, for Case I, when $\epsilon_1 = 0.00125$, n_0 is equal to 904 particles per cell, while when $\epsilon_1 = 0.02$, n_0 is equal to 3395 particles per cell. Table I shows the ratio n_b/n_0 in each simulation.

III. SIMULATION RESULTS

A. Case I: Uniform B_z along $z=0$

We first investigate a current sheet in which B_z is constant ($=\epsilon_1 B_0$) along $z=0$. Fig. 1(a) shows the time-evolution of the contour of the magnetic flux function (the top and middle panels), and B_z along $z=0$ (the bottom panel). In these plots, the mass ratio is $m_i/m_e = 25$ and the magnitude of B_z along $z=0$ is $0.005B_0$ ($\epsilon_1 = 0.005$). Since there is a finite value of B_z at $t=0$, the topology of the magnetic field is not amenable to tearing, and none occurs until $\Omega_i t = 10$ (where Ω_i is the ion cyclotron frequency based on B_0), even though fluctuations in B_z grow in the early stage ($\Omega_i t < 10$). When B_z locally reaches values close to zero around $\Omega_i t = 10$, magnetic islands start to form. At $\Omega_i t = 20$, there are multiple magnetic islands (the middle panel). Fig. 2(a) displays the dependence of the growth rate on the wave number with $\epsilon_1 = 0.0025$, for the mass ratio 25. Results for other mass ratios are qualitatively very similar. The fastest growing mode is around $kw = 0.4$, where k is the wave number, and its growth rate is around $0.2\Omega_i$. The maximum growth rate depends on the mass ratio, and it becomes smaller when the mass ratio is higher.

We have studied the scaling of growth rates with the mass ratio and the magnitude of B_z . Fig. 2(b) shows the dependence of the growth rate (the average between $kw = 0.31$ and 0.5) on the mass ratio, in the runs with $\epsilon_1 = 0.0025$. In the case of small mass ratios, the growth rate does not depend on the mass ratio very much, but in the regime of high mass ratios, the growth rate decreases as the mass ratio increases. The black straight line represents a power law proportional to $(m_i/m_e)^{-1/4}$, and the magnitude of the growth rate is about one-third of the asymptotic electron tearing stability theory,^{1,20} $\gamma = \pi^{1/2}(v_{Te}/w)(\rho_e/2w)^{3/2}[(T_i+T_e)/T_e](1-k^2w^2)$, where v_{Te} and ρ_e are the electron thermal speed and the electron gyro-radius in a magnetic field B_0 , respectively. The overall dependence on the mass ratio in the regime of high mass ratio suggests that the instability is the electron tearing mode. If this were the ion tearing mode, the growth rate γ/Ω_i

TABLE I. The ratio n_b/n_0 .

Case	ϵ_1	n_b/n_0
I	0.00125	0.145
I	0.0025	0.129
I	0.005	0.104
I	0.00707	0.0878
I	0.01	0.0707
I	0.0141	0.0536
I	0.02	0.0387
II ($x=30w$)	0.03	0.0191
II ($x=70w$)	0.03	0.0256

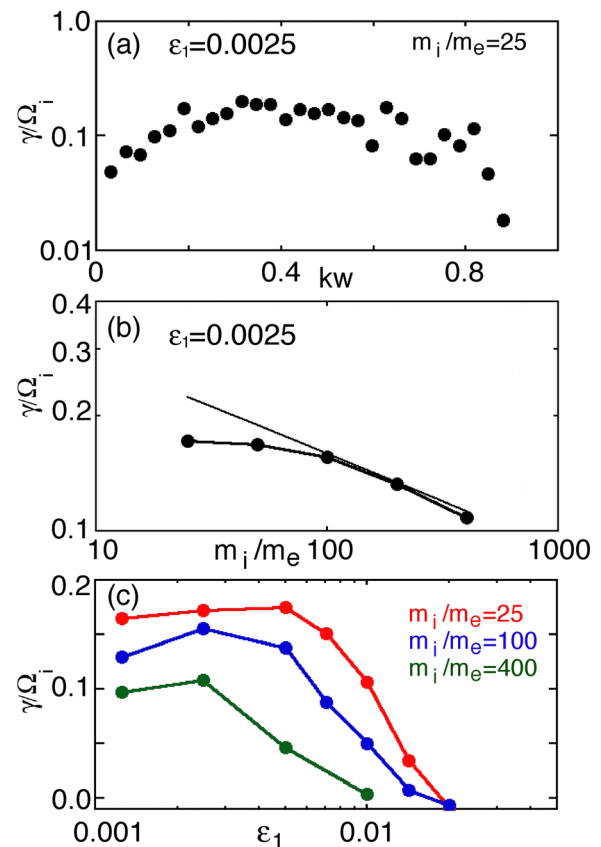


FIG. 2. Dependence of the growth rate in a run of Case I on: (a) the wave number k , (b) the mass ratio, and (c) the magnitude of B_z along $z=0$ ($\epsilon_1 = B_z/B_0$). In (b), the black straight line is $1/3$ of the theoretical value by the asymptotic theory of the electron tearing mode.

would not depend on the electron-to-ion mass ratio.³ We speculate that the systematically smaller growth rates observed in our simulations might be because the current sheet width in our numerical study is of the order of the ion skin depth, which is very thin compared with the current sheet in the asymptotic theory in which the ideal region is assumed to be well separated from the electron and ion kinetic scales. The growth rate of the electron tearing mode is proportional to the value of Δ' ,¹⁰ which represents how large the free energy in the ideal region is. It is possible that Δ' (or available free energy) in the simulation is much smaller than that in the asymptotic theory, because of the thinness of the current sheet.

Figure 2(c) shows the dependence of the growth rate on ϵ_1 , the magnitude of B_z/B_0 . Three colors show results for different mass ratios. In high ϵ_1 regime, the growth rate in each simulation is close to zero, but when ϵ_1 becomes smaller than a certain critical value in each mass ratio, the growth rate increases. In the low ϵ_1 regime, the curve for each mass ratio becomes flat and does not depend on ϵ_1 very much. This tendency is consistent with the argument given by Pellat *et al.*,⁶ who maintain that the tearing mode is unstable when $k\rho_{ez} > 1$, where ρ_{ez} is the electron gyroradius in B_z ($\rho_{ez} = v_{Te}/(eB_z/m_e c)$); in other words, when the wave length becomes smaller than the scale of electron gyro-radius, the electron kinetics becomes important and the tearing mode grows. Using the relations $w = 0.5d_{i0}$, $B_0^2/8\pi = n_0(T_i + T_e)$,

and $T_i = 5T_e$, we obtain $k\rho_{ez} = (2kw/6^{1/2})(m_e/m_i)^{1/2}(1/\epsilon_1)$. If we use $kw = 0.3 - 0.4$, the condition $k\rho_{ez} > 1$ is equivalent to $\sim 0.3(m_i/m_e)^{-1/2} > \epsilon_1$. We see that Fig. 2(c) is qualitatively consistent with this prediction; the critical value of ϵ_1 , below which the tearing mode grows, for the mass ratio 25 is larger than that for the mass ratio 400.

These results are consistent with the conclusion that the unstable wave is the electron tearing mode, where the electron physics causes the instability. Previous studies,^{11,12} discussed the ion tearing mode, and Pritchett¹² interpreted the decrease of the growth rate at high mass ratios as the stabilization of the ion tearing mode by electron physics. However, in that study the dependence of the growth rate on the mass ratio when $k\rho_{ez} > 1$ was not considered. We have done two scaling studies: the first one is on the mass ratio where $k\rho_{ez} > 1$ is satisfied for all the growing waves, and the second one is on the magnitude of B_z , where we found a drop in the growth rate when $k\rho_{ez} < 1$ for different mass ratios. We thus conclude that in these cases, if there is an instability, it is the electron tearing mode, not the ion tearing mode.

B. Case II: Spatially varying B_z along $z = 0$

Next, we have investigated a case in which B_z is spatially varying and has a hump along $z = 0$. In this magnetic field configuration, Sitnov and Schindler¹⁴ have predicted recently that the ion tearing instability can grow. To see if the ion tearing mode grows, we consider the parameter range $k\rho_{ez} \lesssim 1$, where the electron tearing mode is suppressed. Fig. 1(b) shows the time evolution of the magnetic field lines (the top and middle panels), and B_z along $z = 0$ until $\Omega_i t = 24$, where the mass ratio is 100, $\epsilon_1 = 0.03$, $\epsilon_2 = 0.1$, $\alpha = 2.0$, and $x_0 = 30w$ (the location of the peak in B_z). With these parameters, $k\rho_{ez} \lesssim 1$ for modes around $kw \sim 0.4$. Although the electron tearing mode is stable, the bottom panel of Fig. 1(b) shows that instability grows. The peak of the hump is seen to move leftward (earthward), but the dynamics does not cause a reduction of B_z to zero or negative values. Therefore, there is no change of magnetic field-line topology or island formation, and at this initial stage, the instability cannot be described as a tearing mode (see the middle panel of Fig. 1(b), at $\Omega_i t = 24$). The top panel of Fig. 3 shows the time evolution of B_z along $z = 0$ after $\Omega_i t = 24$. The hump of B_z moves further earthward, with its magnitude increasing exponentially. At $\Omega_i t = 42$, a late nonlinear stage of the instability, the B_z field exhibits a negative value behind the hump. Around that time, the tearing instability starts to grow. The middle and the bottom panels of Fig. 3 show the time evolution of the magnetic flux function, and we see that a magnetic island is formed and ejected tailward.

The time-evolution of the system at this late nonlinear stage exhibits a complex character that cannot be attributed to a simple eigenmode. Rather, mode-coupling effects become very important. Fig. 4(a) displays the growth rate of each N mode (N is defined in $k = 2\pi N/L_x$, where L_x is the system length in the x direction, $L_x = 200w$) as a function of time for the simulation with $m_i/m_e = 100$. In the early phase ($\Omega_i t < 25$), the dominant modes are low- N modes ($N < 10$), as shown by the red ($N = 1$), magenta ($N = 7$), and purple

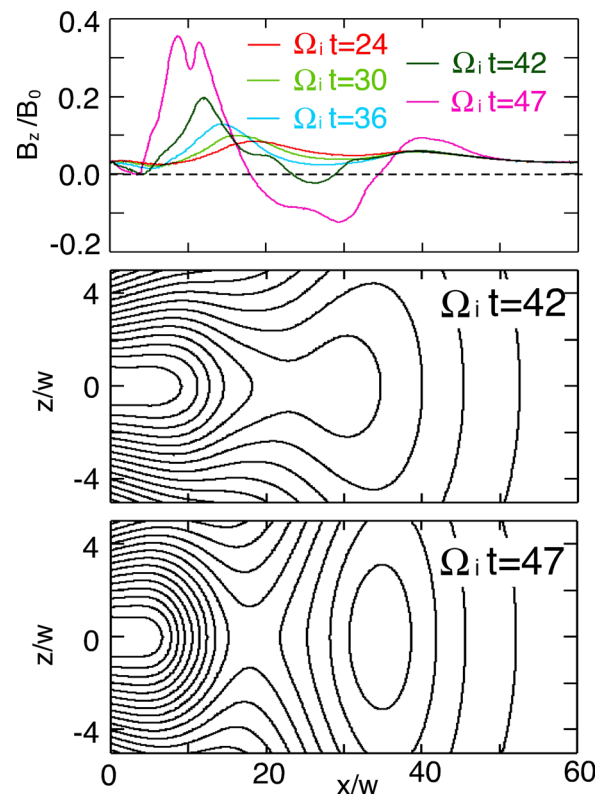


FIG. 3. (Top) time evolution of B_z along $z = 0$ in Case II ($\epsilon_1 = 0.03$, $\epsilon_2 = 0.1$, $\alpha = 2.0$, $m_i/m_e = 100$). (Middle and bottom) contours of magnetic flux function.

($N = 9$) curves in the figure. These modes start to grow linearly after $\Omega_i t \sim 10$, when the initial transient evolution (due to the initial perturbation in E_y explained in Sec. II) ends. In Fig. 4(b), the growth rates of these low- N modes are plotted as the blue curve with closed circles. These modes are expected to be unstable because the instability condition $k < \epsilon_1(4/w\pi)(1 + \alpha)^2 = 0.34/w$ (see the discussion in Sitnov and Schindler,¹⁴ where the instability condition by Lembege and Pellat,⁵ $k < \epsilon_1(4/w\pi)$, is modified by introducing a hump of B_z with $\alpha \neq 0$) is satisfied for $N < 11$.

Higher- N modes ($N > 11$) are stable during the early stage ($\Omega_i t < 25$); however, as shown with the blue and the light blue curves in Fig. 4(a) ($N = 13$ and 14), these modes become unstable after $\Omega_i t \sim 25$. This is likely due to mode-coupling effects, which occur in a large amplitude nonlinear wave and induce the wave steepening. In Fig. 4(b), the triangles in the blue curve are the modes that are destabilized after $\Omega_i t \sim 25$. These modes have larger growth rates than initially unstable modes ($N < 11$). After $\Omega_i t = 35$, much higher- N modes ($N > 18$) start to grow, and these modes have much larger growth rates as shown in the blue curve with squares in Fig. 4(b). These modes ($N > 18$) make further steepening of the hump in B_z , as seen in the top panel of Fig. 3. Eventually with the aid of these high- N modes ($N > 11$), breaking of the magnetic field lines occurs, and a magnetic island behind the hump is formed around $\Omega_i t = 42$.

Figure 4(b) shows the dependence of the growth rate γ in three different mass ratios $m_i/m_e = 25, 100$, and 400. The curves with circles are initially unstable modes ($N < 11$), and they depend weakly on the mass ratio. The growth rates

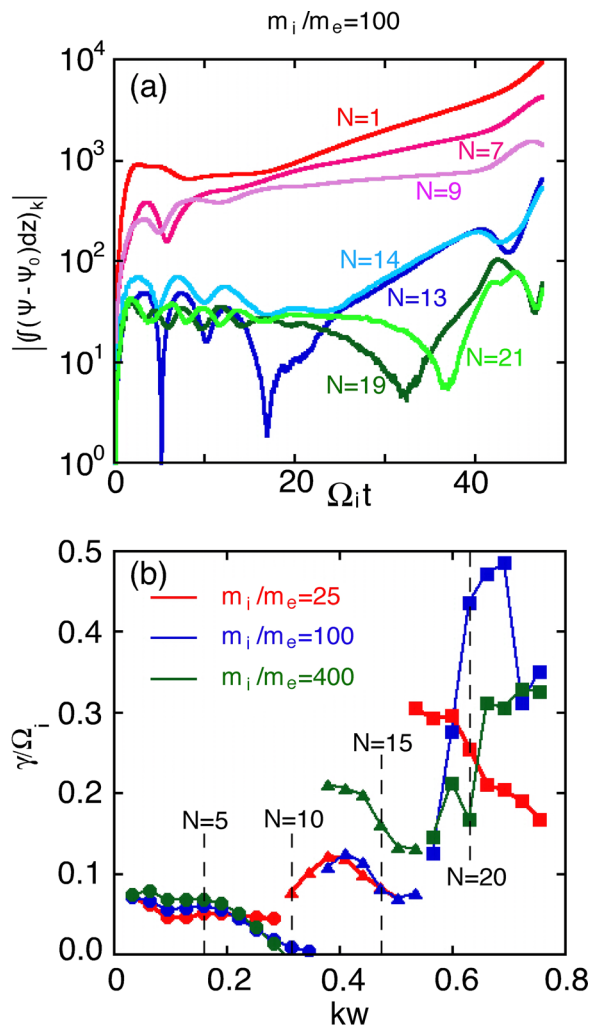


FIG. 4. In a run of Case II ($\epsilon_1 = 0.03$, $\epsilon_2 = 0.1$, $\alpha = 2.0$): (a) the mode amplitude as a function of time ($m_i/m_e = 100$). (b) The growth rate as a function of kw .

increase weakly with the mass ratio ($\gamma/\Omega_i \propto (m_i/m_e)^{0.12}$), which is contrary to the expectations for the electron tearing eigenmode discussed earlier in this paper. The growth rates in the nonlinear stage for $N > 11$ show much larger values. The dependence of these nonlinear growth rate on the mass ratio shows some complication; the growth rates for $m_i/m_e = 400$ in $11 < N < 18$ are larger than those for the other mass ratios, but for higher N -modes with $N > 18$ the growth rates for $m_i/m_e = 100$ show the largest values. While these dependencies are complicated, we expect that this secondary instability associated with a hump in B_z , which has a strong multi-mode character, will play an important role in supporting a dipolarization front even with realistic mass ratio in the Earth's magnetotail.

IV. DISCUSSION AND SUMMARY

We have performed PIC simulations for the instability of a current sheet in the Earth's magnetotail in the presence of a finite B_z . We have demonstrated instability in two types of magnetic configuration. In the case of a uniform B_z along $z=0$ (Case I), we have shown that the relevant instability when B_z is small is the electron tearing mode, not ion tearing.

In the case of spatially varying B_z along $z=0$ (Case II), an instability that is qualitatively different from the electron tearing mode has been observed. The hump of B_z moves earthwards, and a magnetic island is eventually formed in the late nonlinear stage. We note that the hump of B_z is initially located where the current sheet width is around $2.5\rho_{i0}$ (ρ_{i0} : the ion gyro-radius in B_0), and this result is fairly consistent with Sitnov and Swisdak,¹⁵ who observe significant growth when the current sheet width becomes $1.7\rho_{i0}$. Sitnov *et al.*¹⁶ called this the "slippage instability," relating to the ion tearing instability. Although the qualitative features seen in their simulations and ours are quite similar, our physical interpretations are quite different in that we do not describe the underlying linear instability as a tearing mode which must entail a change of topology, not seen in our simulations. Instead, field line breaking occurs in a late nonlinear stage, and eventually a magnetic island is ejected tailward.

As mentioned above, the thickness of the current sheet at the B_z hump plays an important role in the growth of the instability. Pritchett¹⁸ demonstrated that a 2-D current sheet with a hump of B_z is stable. However, in his simulation, the B_z hump is located where the current sheet thickness is more than $6\rho_{i0}$, which is much larger than that in our result and in Sitnov and Swisdak.¹⁵ We have also performed a simulation where the thickness of the current sheet at a B_z hump is $8\rho_{i0}$ (the peak of B_z is located at $x = 70w$; data not shown). In that simulation, no significant growth of the instability as well as the formation of a dipolarization front occurs, but only a slight decay of the hump (20% reduction of the hump) occurs in the early stage (before $\Omega_i t \sim 10$, likely due to departures of the initial equilibrium from perfect force balance). In that simulation, from $\Omega_i t \sim 10$ to the end of the simulation ($\Omega_i t \sim 50$), the profile of the hump of B_z does not change very much and the current sheet is stable. Therefore, we conclude that even in a 2-D case, as Sitnov and Swisdak¹⁵ discussed, a current sheet with a B_z hump is unstable when the thickness of the current sheet at the hump is less than approximately $2\rho_{i0}$.

Whether this instability that shows up in the presence of a hump in B_z is essentially a fluid or a kinetic instability remains an open question. Recently, Zhu *et al.*²¹ discussed instability in the presence of spatially varying B_z along $z=0$ using resistive MHD global simulations, and they have identified a so-called axial tail instability which does not appear to have a tearing character. The magnetic configuration in their study has a dip in B_z , instead of a hump as in our studies. Further studies are necessary to investigate the nature of this instability in both kinetic and fluid models. What complicates this determination is the role played by plasma convection in both kinetic and fluid models, which renders the linear eigenmode problem non-self-adjoint. Under these conditions, the linear stability of the magnetotail cannot be simply described in terms of the standard eigenmodes of a static plasma, and multi-mode effects can exhibit complex transient behavior.

We remark that the instability in the presence of a hump of B_z can lead to the formation of a dipolarization front during a magnetotail substorm without necessarily involving magnetic reconnection. As we see in Fig. 3, a thin, d_i -scale

B_z structure is formed by the instability, even before the magnetic island is formed, due to the steepening of the magnetic structure in the nonlinear stage. Magnetic reconnection occurs after the formation of the dipolarization front, and it is caused by the instability in the late nonlinear stage. The formation of a dipolarization front due to this type of instability is consistent with the picture put forward by Sitnov and Swisdak¹⁵ and Sitnov *et al.*¹⁶ Further analytical and numerical studies are needed in order to elucidate the formation and evolution of the dipolarization front due to the instability and its possible implications for particle acceleration.

In conclusion, we have demonstrated that the Earth's magnetotail exhibits the collisionless electron tearing instability only when the B_z -field is very small or zero. When the B_z -field has a spatial hump, we confirm the existence of an instability discussed by Sitnov and co-workers,^{15,16} but it is not one that tears field lines. In the nonlinear regime, this instability can lead to the formation of a dipolarization front and subsequently to magnetic reconnection when B_z is reduced to very small values or zero. Under no circumstances, do we find the ion tearing instability.

ACKNOWLEDGMENTS

It is a pleasure to acknowledge trenchant discussions with Dr. M. Sitnov on the subject of ion tearing modes, and we thank him for his encouragement to continue with our research on this problem. This work was supported by NSF Grant Nos. ATM-090315 and AGS-1338944, NASA Grant No. NNX09AJ86G, and DOE Grant No. DE-FG02-14-07ER46372, under the auspices of the Center for Integrated Computation and Analysis of Reconnection and Turbulence.

We acknowledge the use of computer resources at the National Energy Research Scientific Computing Center.

- ¹B. Coppi, G. Laval, and R. Pellat, *Phys. Rev. Lett.* **16**, 1207 (1966).
- ²D. Biskamp, R. Z. Sagdeev, and K. Schindler, *Cosmic Electrody.* **1**, 297 (1970).
- ³K. Schindler, *J. Geophys. Res.* **79**, 2803, doi:10.1029/JA079i019p02803 (1974).
- ⁴A. A. Galeev and L. M. Zelenyi, *Sov. Phys. JETP* **43**, 1113 (1976).
- ⁵B. Lembège and R. Pellat, *Phys. Fluids* **25**, 1995 (1982).
- ⁶R. Pellat, F. V. Coroniti, and P. L. Pritchett, *Geophys. Res. Lett.* **18**, 143, doi:10.1029/91GL00123 (1991).
- ⁷F. V. Coroniti, *J. Geophys. Res.* **85**, 6719, doi:10.1029/JA085iA12p06719 (1980).
- ⁸J. Büchner and L. M. Zelenyi, *J. Geophys. Res.* **92**, 13456, doi:10.1029/JA092iA12p13456 (1987).
- ⁹M. Brittnacher, K. B. Quest, and H. Karimabadi, *Geophys. Res. Lett.* **21**, 1591, doi:10.1029/94GL01697 (1994).
- ¹⁰X. Wang and A. Bhattacharjee, *J. Geophys. Res.* **98**, 19419, doi:10.1029/93JA01153 (1993).
- ¹¹P. L. Pritchett, F. V. Coroniti, R. Pellat, and H. Karimabadi, *J. Geophys. Res.* **96**, 11523, doi:10.1029/91JA01094 (1991).
- ¹²P. L. Pritchett, *J. Geophys. Res.* **99**, 5935, doi:10.1029/93JA03297 (1994).
- ¹³B. G. Harrold, A. Bhattacharjee, and X. Wang, *Phys. Plasmas* **2**, 3857 (1995).
- ¹⁴M. I. Sitnov and K. Schindler, *Geophys. Res. Lett.* **37**, L08102, doi:10.1029/2010GL042961 (2010).
- ¹⁵M. I. Sitnov and M. Swisdak, *J. Geophys. Res.* **116**, A12216, doi:10.1029/2011JA016920 (2011).
- ¹⁶M. I. Sitnov, N. Buzulukova, M. Swisdak, V. G. Merkin, and T. E. Moore, *Geophys. Res. Lett.* **40**, 22, doi:10.1029/2012GL054701 (2013).
- ¹⁷N. Bessho and A. Bhattacharjee, *Phys. Plasmas* **14**, 056503 (2007).
- ¹⁸P. L. Pritchett, *Phys. Plasmas* **20**, 080703 (2013).
- ¹⁹C. K. Birdsall and A. B. Langdon, *Plasma Physics via Computer Simulation* (Institute of Physics Publishing, 1991), p. 369.
- ²⁰G. Laval, R. Pellat, and M. Vuillemin, *Plasma Phys. Controlled Fusion Res.* **2**, 259 (1966).
- ²¹P. Zhu, J. Raeder, C. C. Hegna, and C. R. Sovinec, *J. Geophys. Res.* **118**, 653, doi:10.1029/2012JA017972 (2013).